PCCP

ROYAL SOCIETY OF CHEMISTRY

PAPER

View Article Online
View Journal | View Issue

Cite this: *Phys. Chem. Chem. Phys.*, 2024, **26**, 18466

Cross-over from pyrene to acene optical and electronic properties: a theoretical investigation of a series of pyrene derivatives fused with N-, S, and O-containing heterocycles†

Hachem Araji,[a] Maria Nakhoul,[b] Elio Challita,[c] Nour Barmo[a] and Brigitte Wex*[a]

Received 20th April 2024,
Accepted 13th June 2024

DOI: 10.1039/d4cp01625d

rsc.li/pccp

Pyrene and acene derivatives are an important source of materials for optoelectronic device applications both as emitters and organic semiconductors. The mobility of major charge carriers is correlated with the coupling constants of the respective major charge carrier as well as the relaxation energies. Herein, we have applied range-separated density functionals for the estimation of said values. A series of five alkylated derivatives of pyrene laterally extended by heteroaromatic or phenyl groups were explored and contrasted to nascent pyrene, alkylated pyrene and tetracene. The ground state geometries along with absorption properties and relaxation energies are presented as well as a discussion of the suitability of the material toward hole and electron transport materials.

Introduction

Optoelectronic devices encompass photovoltaic cells for energy generation, light-emitting diodes for display applications in smart phones, computers, and televisions, as well as field-effect transistors, which are regulating units. Modern, light-weight, low cost and mass-produced consumer electronics require the use of organic materials based on carbon, hydrogen, oxygen, sulfur, nitrogen, *etc.* to serve as the needed semiconducting materials. In this context, specifically π-conjugated materials like polycyclic aromatics (pyrenes and acenes) as well as heterocyclic aromatics (thiophene, pyrrole, furan, and derivatives thereof) are important building blocks for the design of new organic semiconducting materials.[1–5] Quantum calculations using Density Functional Theory (DFT) computations have become a vital component in the prediction and assessment of new materials to be used as semiconductors,[6] light capturers, and light emitters.[7] DFT calculations are widely used to understand and explain absorption and emission properties,[8] charge-carrier mobilities[9,10] and properties pertaining to electron and hole transfer.[11] Thereby, transfer integral H_{ab} and reorganizational energy (λ) have gained importance as a handle in data-mining approaches combined with machine-learning for material development.[12,13]

Tetracene (**TC**) is a well-characterized material, which shows significant photosensitivity,[14,15] and a bandgap of 2.4 eV.[16] **TC** is thus well-suited for solar energy conversion. The **TC** core serves as the donor building block and semiconductor. **TC** was utilized in field-effect transistors[17,18] and was shown to have a field-effect mobility up to 0.4 $cm^2 V^{-1}s^{-1}$.[19] Substitutions on **TC** by electron-withdrawing groups was explored theoretically.[20] By extension, the linear acene series of polycyclic aromatic hydrocarbons has been a vast arena for exploration of new materials.[21] One approach, the stitching of 2, 3, 4, 5 or more benzene rings along a linear axis following the quest set-out by Clar[22] and others, has culminated in the recent achievement of the synthesis of decacene.[23] Prone to instabilities due to photochemical and oxidative stimuli, what remains challenging in this quest along these synthetic endeavors are approaches to stabilize these acene series by steric and electronic factors. Apart from extension along the linear axis by linear fusions,[24] approaches into the 2[nd] and angular dimension,[25–28] and the embellishment with substituents[29,30] have resulted in stable semiconducting materials.[26,31]

Device performance then is apart from device geometry, preparation, and operational influences – fundamentally governed by the intrinsic mobility of charge carriers. Said carrier mobility in organic semiconductors in turn is determined by

[a] *Lebanese American University, Department of Natural Sciences, Byblos, Lebanon. E-mail: brigitte.wex@lau.edu.lb*
[b] *Lebanese American University, Department of Computer Science and Mathematics, Byblos, Lebanon*
[c] *Lebanese American University, Department of Industrial and Mechanical Engineering, Byblos, Lebanon*

† Electronic supplementary information (ESI) available: Data supporting this article have been included as part of the ESI.† The xyz files of DFT-optimized compounds **1a–e**, **PY**, **2**, and **TC** are available in the SI. See DOI: https://doi.org/10.1039/d4cp01625d

reorganization energies, and thereby the charge-transport rate (*vide supra*).[32] Charge transfer is described by the Marcus electron transfer theory. Therein, the electron transfer rate is a function of Gibbs standard free energy for the reaction, electronic coupling, and reorganization energy.[33,34]

Reorganizational energies were used as a factor in the assessment of charge transfer rate in various optoelectronic materials, for example, azadipyrromethene-based metal complexes for solar cells,[35] heteroatom-bridged benzothiazolyls for organic solar cells,[36] high-performance host materials for phosphors in phosphorescent organic light-emitting diodes (PHOLEDs),[37,38] and OLEDs.[39]

The two fundamental models to describe charge transport are hopping and band-like, the former increasing and the latter decreasing with temperature of the operating environment.[40] Two materials with record-high charge-carrier mobility in single crystals are rubrene and pentacene. Both exhibit band-like transport when tested over a range of hundreds of Kelvin. Herein, we ondulated **TC** into the second dimension with alkyl groups and substitute both terminal phenyl rings along the linear backbone with either thiophene, furan, pyrrole, or thiazole. We apply DFT to shed light on the electronic and optical properties. Herein, we report on four heteroaryl-fused di-*tert*-butyl substituted materials (**1a–d**) as potential new materials for optoelectronic device applications, specifically 2,8-di-*tert*-butylpyreno[4,5-*b*:9,10-*b*′]dithiophene (**1a**),[41] 2,8-di-*tert*-butylpyreno[4,5-*b*:9,10-*b*′]difuran (**1b**), 2,8-di-*tert*-butyl-4,10-dihydropyrrolo[3′,2′:9,10]phenanthro[4,5-*efg*]indole (**1c**), 2,8-di-*tert*-butylpyreno[4,5-*d*:9,10-*d*′]bis(thiazole) (**1d**). Only compounds **1a**, **1c**, and **1d** have previously been proposed or reported in patent applications.[41,42] For compound **1b**, only derivatives were reported.[43] In addition, we report on the all hydrocarbon-derivative 2,9-di-*tert*-butyldibenzo[*fg*,*op*]tetracene (**1e**).[44] Along with this series, pyrene (**PY**),[45] 2,7-di-*tert*-butylpyrene (**2**),[46] and **TC**[47] serve as benchmark hydrocarbons, Fig. 1.

Based on the analysis of possible resonance structures, compound **1e** can be referenced similar to anthracene with 2 moving Clar's sextet, or triphenylene-type with four localized Clar's sextets, Scheme 1.[48,49]

Results and discussion

The molecular geometries of target compounds **1a–1e**, **PY**, **2**, and **TC** were optimized using DFT under the application of the hybrid B3LYP[50] functional and 6-31G(d,p)[51] basis set. Then, the geometries were optimized using tuned, range-separated hybrid ωB97X-D functional[52] and cc-pVTZ[53] basis set, Table S2 and Table S3 (ESI†). The range-separation parameter (ω) was tuned using the ionization potential (IP) tuning procedure[54] and yielded ω values in the order of approximately 0.16 for **1a**, **1c**, **1d**, **1e** and slightly higher for **TC** as shown by Bhatta for short, conjugated systems.[16] Values closer and above the default value ω of 0.200[52] were determined for **1b** of 0.24 and **PY** of 0.3, Table 1.

Gas phase photoelectron spectroscopy data revealed IP of 7.41 eV for **PY**[22] and 6.97 eV (^2A_u) for **TC**[55] indicating maximal deviation errors of 5% and below for **PY** and **TC** at this level of theory compared to experimental data. All compounds **1a–e** have IPs in the range of **TC** rather than **PY**, whereby it is noted that the substitution of the 2,7-positions with *tert*-butyl groups on **PY** to obtain **2** most substantially effects the IP by 0.5 eV. This is a larger factor than the lateral fusion with phenyl groups when going from compound **2** to **1e**. IPs of **1b**, **1c**, and **TC** are closest around 6.60 eV. The higher electronegativity of the heteroatom (O > N > S) in its role to stabilize the HOMO

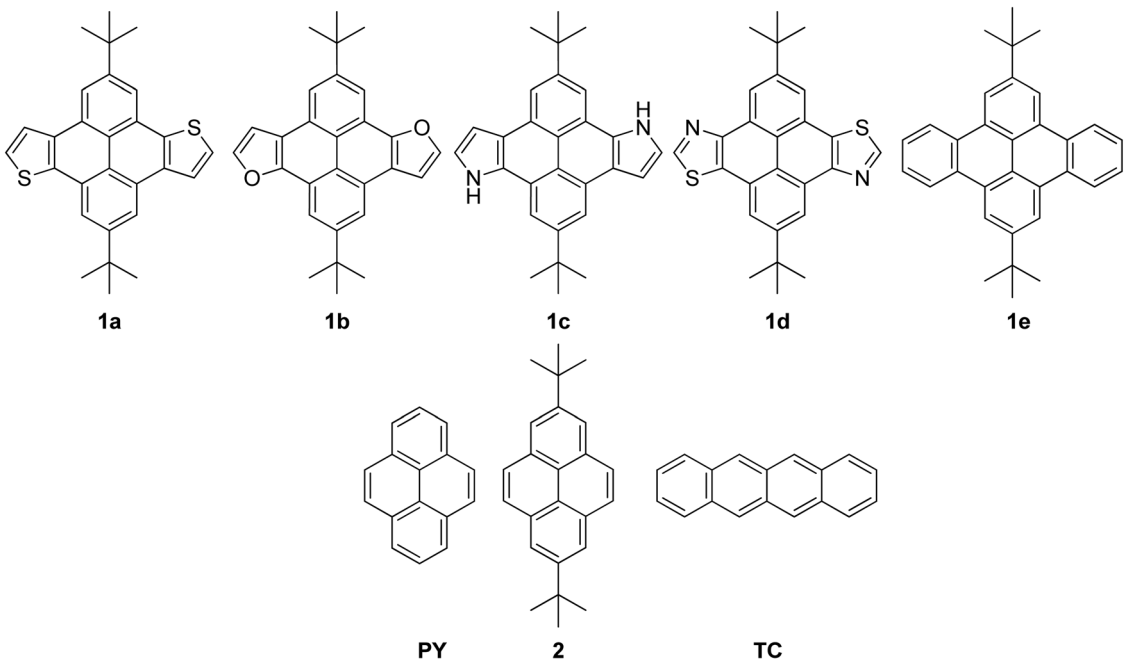

Fig. 1 Overview of materials of interest, **1a–e** along with reference compounds **PY**, **2**, and **TC**.

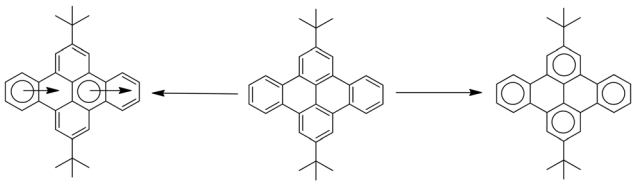

Scheme 1 Analysis for Clar's sextet in compound **1e**.

level[56] and increasing the ionization potential shows herein a minuscule effect of 0.2–0.3 eV and no effect in the case of thiazole **1d** compared to compound **1e**, respectively. In other words, a modification of a phenyl unit to a thiophene, furan, or pyrrole lowers the IP by 0.2 to 0.4 eV, while the modification to a thiazole unit shows no effect on the IP.

In addition, the solid state ionization potential and the electron affinity are often approximated by cyclic voltammetry experiments.[57] For example, the ionization potential of **PY** is determined at 1.3 V *vs.* SCE.[58] Hansen reported the absolute potential for SCE as 4.698 eV.[59] Therefore, the IP for **PY** converts to 6.0 eV. The IP of **TC** is reported as 0.72 V *vs.* SCE,[60] which converts to 5.42 eV. Similarly, we report the oxidation potential of **2** to yield 5.5 eV based on cyclic voltammetry data, Fig. S1 (ESI†).

EA varies substantially ranging from 0.01 to 0.65 across compounds **1a–e**, however, the values are not approaching the low value as **TC**. Thiophene and thiazole-fused pyrene units **1a** and **1d** have the lowest EA, not surprising since indole itself has an EA of 0.00351 eV.[61] The substitution of **PY** with alkyl groups and then extension to four linearly fused phenyl ring backbone as observed in **1e** has only a minimal effect on the EA level, Table 2. It is noted that for charged species, such as anions as well as for determining electron affinity, the inclusion of diffuse functionals in the level of theory is recommended to capture tail behavior of molecular orbitals[62] as exemplified in other works characterizing the of acene series.[63,64]

Table 2 Ionization potential (IP),electron affinity (EA), and fundamental he gap (E_{fund}) as determined at the ωB97X-D[52]/cc-pVTC[53] level of theory and experimental data for **1a–e**, **PY**, **2**, and **TC**

	IP[a] [eV]	PES[b] [eV]	IP[c]	EA [eV]	EAS[d] [eV]	E_{fund}[e]
1a	6.74	—	—	0.52	—	6.22
1b	6.63	—	—	0.29	—	6.34
1c	6.52	—	—	0.01	—	6.51
1d	6.91	—	—	0.65	—	6.26
1e	6.92	—	—	0.36	—	6.56
PY	7.36	7.41[22]	6.0[58]	0.44	0.59[65]	6.92
2	6.84	—	5.5[f]	0.38	—	6.46
TC	6.60	6.97[55]	5.4[60]	1.02	1.058[66]	5.58

[a] IP and EA were computed by the difference of the total energy of the relaxed cation state and the relaxed ground state or the latter with relaxed anion state, respectively. [b] As determined by gas-phase photoelectron spectroscopy (PES). [c] Determined by cyclic voltammetry with conversion of E_{abs}(SCE) = 4.698 eV. [d] As determined by Electron attachment spectroscopy (EAS).[61] [e] Difference between IP and EA. [f] As determined by cyclic voltammetry.

Absorption properties

Time-dependent Density Functional Theory (TD-DFT) was carried out at tuned, range-separated hybrid ωB97X-D functional[52] and cc-pVTZ[53] basis set for level of theory. The first ten excited states in the series of compounds were computed. Data was analyzed using Gaussum and is presented in Fig. 2. For brevity and relevance, only excitations to S_1 and S_2 are shown below, Table 3. The complete data for all ten excited states of the compound series is presented in Tables S4–S8 (ESI†). While ωB97X-D is known to overestimate the exited state energy level S_1 (^1L_b) in **PY**[67,68] leading to a narrow albeit correct ordering of the first two excited states, the modeled oscillator strengths match experimental observations.[69] Particularly for **PY** the ordering of excited states is often observed as wrong, particularly when using TD-DFT. This observation was investigated by Graef and Martins utilizing a large range of functionals with the Def-2svp basis set. When utilizing the functional ωB97X-D, a correlation between changes in geometry and band ordering was drawn utlizing the value of Ω as a function of ω. The parameter Ω is defined as the ratio between the average length of bonds transversal to the central bond in pyrene and the average length of the bonds parallel to the central bond in pyrene, Table S1 (ESI†). In this limited case, the long-range correction along with the optimized geometry had an impact on the band ordering. Thus, correct ordering of the first two states was observed when the value of $\Omega > 1.020$ as verfied using CCSD and MP2 computations. However, an underestimation of the absorption wavelength was observed with the functional ωB97X-D[70] since **PY** exhibits an absorption maximum at 370 nm (extinction coefficient 1.2×10^2 $M^{-1}cm^{-1}$),[71] compound **2** absorbs at 339 nm (dichloromethane),[72] and **TC** (denoted as naphthacene in literature) absorbs at 471 nm (benzene, extinction coefficient 1.0×10^4 $M^{-1}cm^{-1}$)[71] in comparison to the computed values of 293 nm, 317 nm, and 440 nm (this study). Thus, the error ranged from 0.9 eV for **PY** to 0.3 eV for **2** and 0.2 eV for **TC** when comparing solution to gas phase data.

The quantum-mechanical transition dipole moment bridges the gap to the oscillator strength in classical observation.[73] When considering the transition dipole moment, two absorber-types are distinguished herein, the pyrene-type (**PY**-type) and tetracene-type (**TC**-type). Characteristically for **PY**-type, the $S_2 \leftarrow S_0$ absorption band has a transition dipole moment significantly larger than for the $S_1 \leftarrow S_0$.[67,69] Characteristic is the 1 : 1 weighted configurational interaction between H−1 → LUMO and H → LUMO-1 for the lowest energy transition, while configurational interactions between HOMO → LUMO

Table 1 Tuned ω-values ($Bohr^{-1}$) for range-separated hybrid functional ωB97X-D[52] with cc-pVTC[53] basis set for **1a–e, PY**, **2**, and **TC**

Compound	**1a**	**1b**	**1c**	**1d**	**1e**	**PY**	**2**	**TC**
Tuned ω value	0.1564	0.2376	0.1564	0.1564	0.1564	0.3282	0.1564	0.1719

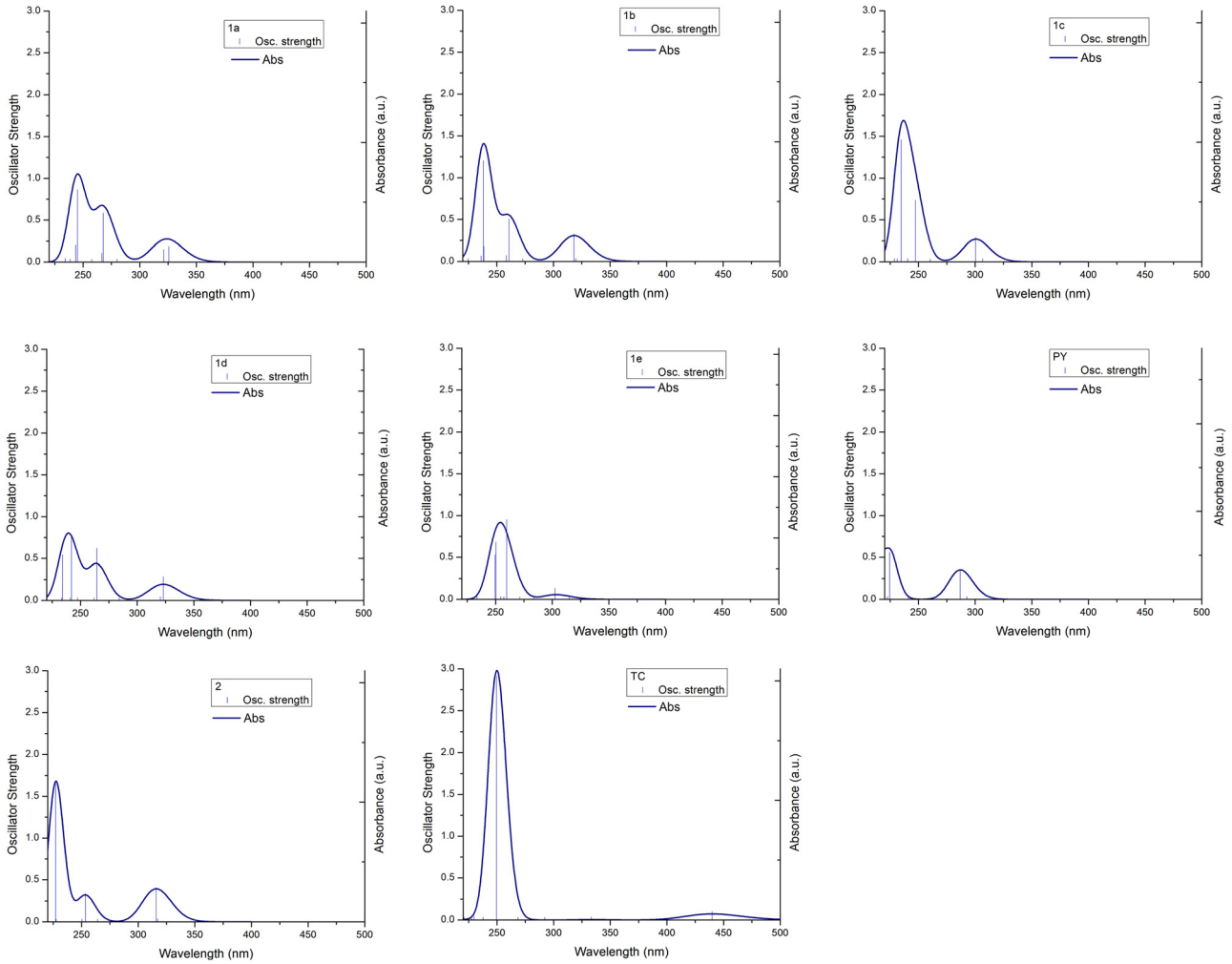

Fig. 2 Oscillator strength and absorption for **1a–e**, **PY**, **2**, **TC** modeled with ωB97X-D functional[52] and cc-pVTZ[53] basis set for level of theory in gas phase.

dominate in the higher energy component.[74] For **TC**-type, the $S_1 \leftarrow S_0$ absorption band has a transition dipole moment significantly larger for than $S_2 \leftarrow S_0$. According to our calculation results obtained at the ωB97X-D[52]/cc-pVTZ[53] level of theory, compounds **1b**, **1c**, **1e** along with **PY** and **2** represent **PY**-type absorbers. For all these cases, the HOMO–LUMO (HL) transition accounts for >75%. Compounds **1a–d** have transition dipole moments significantly larger than **TC**. Compounds **1a** and **1d** exhibit **TC**-type absorption character. However, only **1d** shows the signatory absorption band with HOMO–LUMO contribution of >80%.

Table 3 Gas phase vertical transition energies (E_{vert}, eV), wavelengths (λ_{vert}, nm), oscillator strength (f), transition dipole moments (μ_{ge}, Debye) as computed using time-dependent DFT (TD-DFT) at the ωB97X-D[52]/cc-pVTZ[53] level of theory for **1a–1e**, **PY**, **2**, and **TC**

	Transition			E_{vert}	λ_{vert}	f	μ_{ge}
1a	S_0	→	S_1	3.81	326	0.153	1.642
	S_0	→	S_2	3.86	321	0.117	1.235
1b	S_0	→	S_1	3.88	320	0.004	0.042
	S_0	→	S_2	3.90	318	0.293	3.064
1c	S_0	→	S_1	4.04	307	0.006	0.056
	S_0	→	S_2	4.13	300	0.255	2.519
1d	S_0	→	S_1	3.84	323	0.253	2.688
	S_0	→	S_2	3.87	320	0.013	0.139
1e	S_0	→	S_1	3.93	315	0.012	0.129
	S_0	→	S_2	4.10	302	0.099	0.989
PY	S_0	→	S_1	4.24	293	0.0003	0.003
	S_0	→	S_2	4.32	287	0.325	3.065
2	S_0	→	S_1	3.91	317	0.004	0.045
	S_0	→	S_2	3.92	316	0.378	3.927
TC	S_0	→	S_1	2.82	440	0.07	1.016
	S_0	→	S_2	3.72	333	0.004	0.039

Natural transition orbitals (NTOs)[75,76] of compounds **1a–e**, **PY**, **2**, and **TC** were carried out in an effort to identify if just a single occupied (hole) and unoccupied (particle) NTO pair characterizes the nature of the first and second optically active singlet excited states. The eigenvalues for these transitions are listed in Table 4 and representative NTO pairs are shown in Tables S9–S11 (ESI†). This analysis revealed that only the **TC** $S_1 \leftarrow S_0$ transition is completely described by a single NTO pair with eigenvalue of 0.99 while **1a** and **1d** have eigenvalues for this transition of ≥0.8. The dominating particle for **PY** type transition in $S_2 \leftarrow S_0$ is observed for **1b**, **1c**, **1e**, **PY**, and **2** with eigenvalues of ≥0.76. All frontier highest occupied transition

Table 4 NTO analysis of eigenvalues for NTO pairs based in $S_0 \rightarrow S_1$ and $S_0 \rightarrow S_2$ transitions at the ωB97X-D[52]/cc-pVTZ[53] level of theory for **1a–1e**, **PY**, **2**, and **TC**

	Hole $S_0 \rightarrow S_1$	Particle	Hole $S_0 \rightarrow S_2$	Particle
1a	H−1 (0.16) H (0.82)	L + 1 (0.16) L (0.82)	H−1 (0.22) H (0.76)	L + 1 (0.22) L (0.76)
1b	H−1 (0.40) H (0.58)	L + 1 (0.40) L (0.58)	H−1 (0.11) H (0.89)	L + 1 (0.11) L (0.89)
1c	H−1 (0.39) H (0.58)	L + 1 (0f.39) L (0.58)	H−1 (0.15) H (0.82)	L + 1 (0.15) L (0.82)
1d	H−1 (0.10) H (0.89)	L + 1 (0.10) L (0.89)	H−1 (0.38) H (0.6)	L + 1 (0.38) L (0.6)
1e	H−1 (0.36) H (0.60)	L + 1 (0.36) L (0.60)	H−1 (0.21) H (0.74)	L + 1 (0.21) L (0.74)
PY	H−1 (0.44) H (0.53)	L + 1 (0.44) L (0.53)	H−1 (0.13) H (0.85)	L + 1 (0.13) L (0.85)
2	H−1 (0.42) H (0.57)	L + 1 (0.42) L (0.57)	H−1 (0.10) H (0.90)	L + 1 (0.10) L (0.90)
TC	H (0.99) —	L (0.99) —	H−1 (0.45) H (0.52)	L + 1 (0.45) L (0.52)

H = occupied NTO, L = virtual NTO wherein H and L have the same eigenvalue.

orbital (HOTO) and lowest unoccupied transition orbital (LUTO) molecular orbital pictures of relevant transitions for $S_1 \leftarrow S_0$ and $S_2 \leftarrow S_0$ transitions were analyzed and are shown in Fig. S11–S13 (ESI†). Therein it becomes apparent that the TD-DFT results for this group of compounds are dominated by more than one relevant NTO pair. Elevating the level of theory to describe these polycyclic aromatic hydrocarbons, particularly acenes[77–81] and higher acenes[69] with a combined DFT multi-reference configurational interaction (DFT/MRCI) method exemplifies the complexity of these systems with multireference character and remains to be explored for the presented series.

According to the potential energy surface, the reorganizational energy of going from a neutral ground state to a charged ionic state (cation, anion) requires geometry relaxations.[82] The sum of said terms add up to the total reorganizational energy, which among other factors ultimately has an impact on charge carrier mobility and thus device performance. Using DFT and the Dushin program by Reimers,[83] we have assessed the reorganizational energies of compounds **1a–e**, **PY**, **2**, and **TC** at the ω-tuned ωB97X-D[52]/cc-pVTZ[53] level of theory in this series, Tables 5 and 6.

The calculations completed to assess reorganizational energies upon going from the neutral ground state to the anionic state showed that all five compounds exhibit reorganizational energies ranging from 0.2 to 0.3 eV. The highest value was observed for the compound containing the electronegative atom nitrogen, **1c** with a value closest to pyrene. The remaining are around ∼100 meV lower in reorganizational energy compared to pyrene, Table 5. In comparison to **TC**, the reorganizational energies are on average 24% higher and for **1a–d** all higher than the benzofused derivative

Table 5 Reorganizational energies of target compounds **1a–e**, **PY**, **2**, and **TC** upon going from the neutral to the anionic state at the ωB97X-D[52]/cc-pVTZ[53] level of theory

Compound Neutrl to ANION	$\lambda^{(1)}_{rel}$ meV	$\lambda^{(2)}_{rel}$ meV	λ_{Tot} meV	λ_{Tot} meV —
1a	124	123	247	—
1b	137	137	274	—
1c	154	152	306	—
1d	119	118	237	—
1e	98	121	219	—
PY	192	191	383	—
2	142	142	284	—
TC	106	109	215	151[20 a] 160[84 a]

λ Reorganizational energies. [a] λ_{Tot} meV for **TC** reported at B3LYP/6-31G(d,p) level of theory.

Table 6 Reorganizational energies of target compounds **1a–e**, **PY**, **2**, and **TC** at the ωB97X-D[52]/cc-pVTZ[53] level of theory

Compound Neutral to CATION	$\lambda^{(1)}_{rel}$ meV	$\lambda^{(2)}_{rel}$ meV	λ_{Tot} meV	λ_{Tot} meV —
1a	97	97	194	—
1b	92	92	185	—
1c	107	106	213	—
1d	100	100	200	—
1e	99	98	198	—
PY	154	153	307	—
2	112	112	223	—
TC	83	85	167	107[20 a] 113[84 a]

λ Reorganizational energies. [a] λ_{Tot} meV for **TC** reported at B3LYP/6-31G(d,p) level of theory.

1e. Therefore, in this series, **1e** is the most suitable candidate with only 2% higher reorganizational energy compared to **TC**.

The calculations completed to assess reorganizational energies upon going from the neutral ground state to the cationic state showed that all five compounds **1a–e** exhibit similar values of reorganizational energies. All compounds showed a significantly lower reorganizational energy compared to **PY**, Table 6. In comparison to **TC**, the reorganizational energies are on average 19% higher. Interestingly here, though, is the fact that the reorganizational energies of **1a** and **1b** are 2% and 7% lower compared to **1e**, respectively. This allows the hypothesis that replacing a benzene unit with a heterocyclic aromatic thiophene or furan, allows lowering the reorganizational energies in these types of compounds. Specifically, we have replaced an aromatic C=C bond with a –S– (**1a**) or –O– (**1b**). It was previously shown using photoelectron spectroscopy, that sulfur atom therein behaves like the C=C bond and donates the necessary two electrons to the aromatic system,[85] rendering **1a** and **1b** isoelectronic to **1e**. Due to the lowest value, **1b** is most suitable system from a reorganizational energy point of view.

While there is a survey of omega values applied to **TC** in literature, no tuning of omega is reported on the functional ωB97X-D.[16] The reorganizational energy of **TC** at the B3LYP/6-31G(d,p) level of theory is 107 meV by summing up the

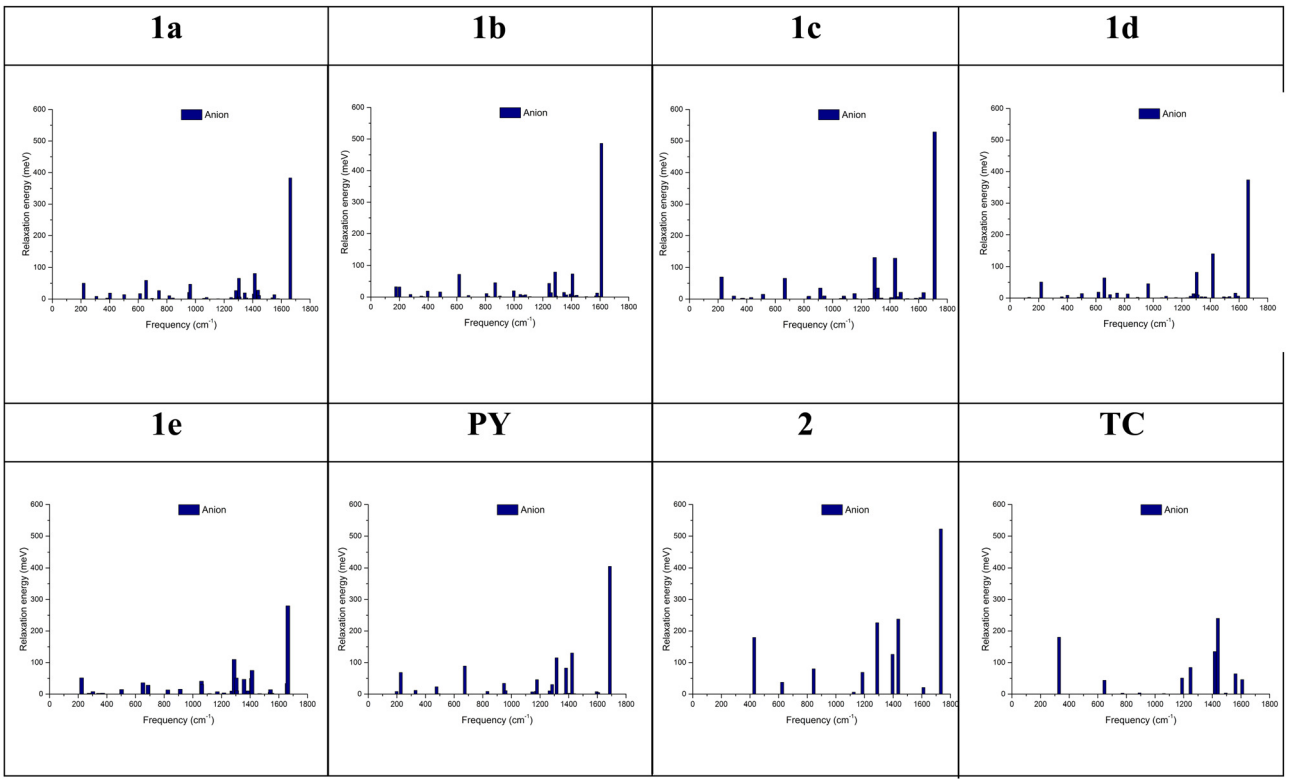

Fig. 3 Vibrational modes observed for the anionic relaxation energy for **1a–d** (up) and **1e**, **PY**, **2**, and **TC** (down). Calculations were completed at the ωB97X-D[52]/cc-pVTZ[53] level of theory.

reorganization energies from the individual normal modes. Rossi reported reorganizational energies of the former type as 117 meV for **TC** using B3LYP/6-31G(d,p) level of theory.[86]

It is noted that the global hybrid functional B3LYP with a fixed, 20% amount of Hartree–Fock (HF) component is known to introduce a many-electron self-interaction error.[87,88]

The minimization of this error is mitigated by the use of range-separated hybrid functionals (LRC) such as ωB97X,[89] and the revised version ωB97X-D, which includes empirical atom–atom dispersion corrections[90] leading to the observed differences in reorganizational energies at these different levels of theory.

Normal mode analysis was completed to elucidate how individual normal modes are contributing to the total reorganization energy. Both the cation and anion relaxational energies were thus dispersed into the individual components under the application of the Dushin program by Reimers.[83] **TC** was previously characterized by the absence of frequencies below 1000 cm^{-1} toward the reorganizational energy.[82]

For the anionic relaxation energy all tabulated results are presented in Tables S12–S19 (ESI†). Specifically, one dominant vibrational mode is located above 1600 cm^{-1} for **1a–e**, **PY**, and **2**. This frequency mode is attributed to the C=C stretching vibration of the aromatic core as visualized by GaussView. Only **1e** is characterized by a low contribution and only **TC** is characterized again by absence of this mode, Fig. 3.

For the cationic relaxation energy all tabulated results are presented in Tables S20–S27 (ESI†). It is noted that the dominant vibrational modes are again located above 1600 cm^{-1} for all compounds except **TC**. As previously observed at the B3LYP/6-31G(d,p) level of theory, only few modes are active in **TC** rending the prediction of mobility to 0.67 $cm^2 V^{-1}s^{-1}$ in a band-like transport mechanism.[40] Specifically for **TC** single crystal, hole mobility reaches values close to $\mu \simeq 1\,cm^2\,V^{-1}\,s^{-1}$ at room temperature from both, time of flight and *I–V* measurements.[91] This high frequency mode is attributed to the C=C bond stretching vibration, Fig. 4, of the aromatic core attributed to bandlike behavior for the mobility.[40]

In contrast to the others, **1e** is characterized by the smaller contribution of this high-frequency band and a higher number of modes across the entire energy range of 200–1700 cm^{-1}.

Conclusions

The modulation of the lateral chain of aromatics into heterocycles has a smaller effect on the IP when compared to substitution by alkyl groups. The EA is vastly influenced by the type of heterocyclic aromatic core used. The computational assessment of cationic reorganizational energies showed that the lateral fusion of heterocycles on pyrene narrowed the material's properties to the related tetracene compound. This effect was only mildly observed for anionic reorganizational energies. Normal-mode analysis using Dushin program revealed C=C stretching to be the major contributor to large reorganizational energies for all except **1e**.

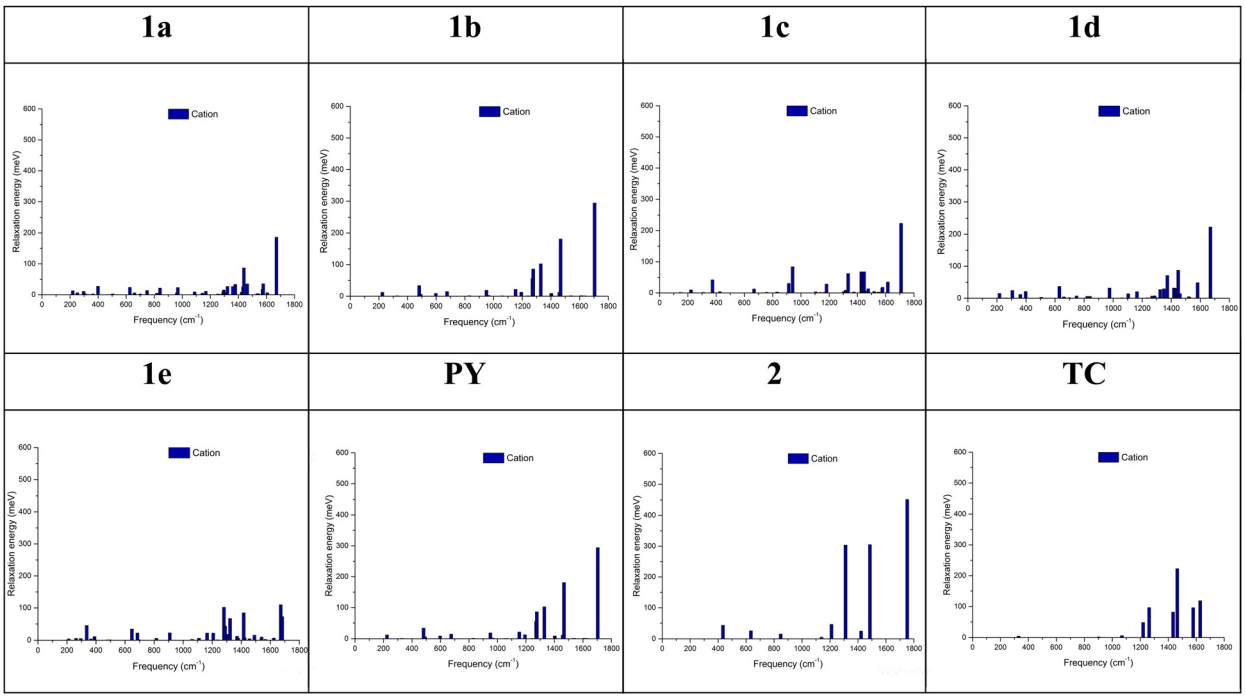

Fig. 4 Vibrational modes observed for the cationic relaxation energy for **1a–d** (up) and **1e**, **PY**, **2**, and **TC** (down). Calculations were completed at the ωB97X-D[52]/cc-pVTZ[53] level of theory.

Materials and methods

Quantum chemical calculations

All calculations were carried out using Gaussian09 (Revision D.01) and visualized using GaussView (Version 5.0.9).[92] Compound structures were drawn in 2D using ChemDraw, converted to 3D using Chem3D module and energy was minimized using MM2 Chem3D (15.0). The geometries were distorted from planarity with ~2–5° dihedral angles using GaussView and geometries were optimizations in the gas phase at the B3LYP/6-31G(d,p) level of theory. The achieved minima were verified by analysis of harmonic vibrational frequencies and verified by the absence of imaginary frequencies. Range-separated functional ωB97X-D[52] was utilized along with the cc-pVTZ[53] basis set with a tuned range-separation parameter ω. This parameter was tuned with the ionization potential (IP) tuning procedure[54] as listed in Table 1 and was utilized for optimization and frequency analysis. The absence of negative frequencies was confirmed.

TD-DFT calculations were carried out and reported at the tuned ωB97X-D[52]/cc-pVTZ[53] level of theory and processed using GAUSSUM3.0.[93]

Electrochemistry

Non-aqueous reference silver wire electrode along with platinum wire counter electrode and glassy carbon working electrode were used in a solution of tetra-*n*-butylammonium hexafluorophosphate (0.1 M) in dichloromethane. Ferrocene (Fc) was used as internal standard. A scan rate of 0.1 V^{-1} s^{-1} with 1×10^{-5} A V^{-1} sensitivity was used.

Reorganizational energies

Total reorganizational energies are the sum of the individual reorganizational energies for going from the neutral geometry to the cation or anion, respectively. Details for the procedure are outlined elsewhere.[34,82,94] In short, the reorganization energy λ is computed as per eqn (1):

$$\lambda = \lambda_1 + \lambda_2 = \left[E_{\pm}^{*} - E_{\pm}\right] + \left[E^{*} - E\right] \quad (1)$$

Herein, E and $E_{\pm}$ are the lowest energy structure of the neutral and cation/anion geometry, respectively, while E^{*} and $E_{\pm}^{*}$ represent the energies of the neutral and cation/anion structure at the vertical transition from the cation/anion and neutral structure, respectively.

Relaxational energies

Relaxational energy λ[82,84,95] and Huang–Rhys factors S_j were computed along a scan across the vibrational modes ω_i under the application of the Dushin program provided by Reimers.[83] The reorganizational energy is thus the sum of each vibrational mode as outlined in eqn (2) and this was carefully reviewed by Hsu.[34]

$$\lambda = \Sigma\lambda_i = \Sigma S_i \hbar\omega_i \quad (2)$$

Since the analysis herein explores trends rather than absolute values, no scaling was done. Shall a scaling be desired, the computational data is recorded in the ESI† and a scaling of harmonic frequencies with a factor of 0.956 ± 0.002 for ωB97X-D[52]/cc-pVTZ[53] as reported by the Computational Chemistry Comparison and Benchmark DataBase may be applied.[96]

Data availability

Codes Gaussian09 Revision D.01 and GaussView (Version 5.0.9) were purchased from Gaussian and used as received. Gaussum was downloaded from the website.[93] Dushin code[83] was provided by Prof. Reimers following email communication.

Conflicts of interest

There are no conflicts to declare.

Acknowledgements

B.W. is grateful for helpful discussions with Prof. Jean-Luc Brédas, Dr. Slava Coropceanu, Dr. Alexandr Fonari and Dr. Zilong Zheng. We thank Dr. Jean Takchi and Mr. Gaby El-Alam for writing scripts assisting data processing, as well as Mr. Jalal Possik and Mr. Elie Akoury for help in software installations. We acknowledge the PACE Cluster at Georgia Institute of Technology and the LAU Academic Computing Center Server. Financial support from Arab Fund for Economic and Social Development, National Council for Scientific Research (CNRS), the Royal Society of Chemistry (RSC) Research Fund and LAU School of Arts and Sciences Research and Development Fund for the PI are greatly appreciated.

References

1 N. Nicolaus, P. T. Franke and M. Lautens, *Org. Lett.*, 2011, **13**, 4236–4239.
2 I. Osaka, T. Abe, S. Shinamura and K. Takimiya, *J. Am. Chem. Soc.*, 2011, **133**, 6852–6860.
3 K. Niimi, S. Shinamura, I. Osaka, E. Miyazaki and K. Takimiya, *J. Am. Chem. Soc.*, 2011, **133**, 8732–8739.
4 G. D. Lilly, A. C. Whalley, S. Grunder, C. Valente, M. T. Frederick, J. F. Stoddart and E. A. Weiss, *J. Mater. Chem.*, 2011, **21**, 11492–11497.
5 S. Shinamura, I. Osaka, E. Miyazaki, A. Nakao, M. Yamagishi, J. Takeya and K. Takimiya, *J. Am. Chem. Soc.*, 2011, **133**, 5024–5035.
6 G. Gryn'ova, K.-H. Lin and C. Corminboeuf, *J. Am. Chem. Soc.*, 2018, **140**, 16370–16386.
7 A. P. Bella, R. V. Solomon, S. A. Vedha and J. P. Merlin, *Theor. Chem. Acc.*, 2019, **138**, 53.
8 J. Casado, M. Z. Zgierski, M. C. R. Delgado, J. T. L. Navarrete, M. Mas-Torrent and C. Rovira, *J. Phys. Chem. C*, 2007, **111**, 10110–10118.
9 H. X. Li, R. H. Zheng and Q. Shi, *J. Phys. Chem. C*, 2012, **116**, 11886–11894.
10 P. Prins, F. C. Grozema and L. D. A. Siebbeles, *J. Phys. Chem. B*, 2006, **110**, 14659–14666.
11 F. L. Liu, E. Proynov, J. G. Yu, T. R. Furlani and J. Kong, *J. Chem. Phys.*, 2012, **137**, 114104.
12 C. Kunkel, C. Schober, J. T. Margraf, K. Reuter and H. Oberhofer, *Chem. Mater.*, 2019, **31**, 969–978.
13 C. Schober, K. Reuter and H. Oberhofer, *J. Phys. Chem. Lett.*, 2016, **7**, 3973–3977.
14 J. Gundlach, L. Zhou, J. A. Nichols, J.-R. Huang and T. J. Jackson, *Proc. IEEE*, 2001, **34**, 743.
15 R. Signerski and J. Kalinowski, *Thin Solid Films*, 1984, **121**, 175–199.
16 R. S. Bhatta, G. Pellicane and M. Tsige, *Comput. Theor. Chem.*, 2015, **1070**, 14–20.
17 J. Gundlach, J. A. Nichols, L. Zhou and T. N. Jackson, *Appl. Phys. Lett.*, 2002, 80.
18 L. A. Morrison, D. Stanfield, M. Jenkins, A. A. Baronov, D. L. Patrick and J. M. Leger, *Org. Electron.*, 2016, **33**, 269–273.
19 R. W. I. de Boer, T. M. Klapwijk and A. F. Morpurgo, *Appl. Phys. Lett.*, 2003, **83**, 4345–4347.
20 R. Oshi, S. Abdalla and M. Springborg, *Comput. Theor. Chem.*, 2018, **1128**, 60–69.
21 M. Stępień, E. Gońka, M. Żyła and N. Sprutta, *Chem. Rev.*, 2017, **117**, 3479–3716.
22 E. Clar and W. Schmidt, *Tetrahedron*, 1976, **32**, 2563–2566.
23 J. Kruger, F. Garcia, F. Eisenhut, D. Skidin, J. M. Alonso, E. Guitian, D. Perez, G. Cuniberti, F. Moresco and D. Pena, *Angew. Chem., Int. Ed.*, 2017, **56**, 11945–11948.
24 P. Hu, J. Ye and H. Jiang, *J. Mater. Chem. C*, 2019, **7**, 5858–5873.
25 Y. Cao, Y. Liang, L. Zhang, S. Osuna, A. L. M. Hoyt, A. L. Briseno and K. N. Houk, *J. Am. Chem. Soc.*, 2014, **136**, 10743–10751.
26 L. Zhang, A. Fonari, Y. Liu, A. L. M. Hoyt, H. Lee, D. Granger, S. Parkin, T. P. Russell, J. E. Anthony, J. L. Brédas, V. Coropceanu and A. L. Briseno, *J. Am. Chem. Soc.*, 2014, **136**, 9248–9251.
27 E. K. Burnett, J. Ly, M. R. Niazi, L. Zhang, S. R. McCuskey, A. Amassian, D.-M. Smilgies, S. C. B. Mannsfeld and A. L. Briseno, *Adv. Mater. Interfaces*, 2018, **5**, 170161–170168.
28 M. Rosenkranz, L. Graf, B. Büchner, M. Knupfer and A. A. Popov, *J. Mater. Chem. C*, 2023, **11**, 12714–12729.
29 X. Zhang, L. Jiang, H. Dong, X. Lu, H. Geng, R. Li and W. Hu, *J. Photochem. Photobio. A*, 2018, **355**, 131–135.
30 G.-Y. Qin, X.-Q. Sun, P.-P. Lin, X. Wei, J.-F. Guo, W.-B. Cui, J.-X. Fan, H. Li, L.-Y. Zou and A.-M. Ren, *J. Mater. Chem. C*, 2023, **11**, 13018–13029.
31 L. Zhang, Y. Cao, N. S. Colella, Y. Liang, J. L. Brédas, K. N. Houk and A. L. Briseno, *Acc. Chem. Res.*, 2015, **48**, 500–509.
32 J. M. Granadino-Roldan, A. S. Garzon, G. Garcia, M. N. Moral, A. Navarro, M. P. Fernandez-Liencres, T. S. Pena-Ruiz and M. Fernandez-Gomez, *J. Phys. Chem. C*, 2011, **115**, 2865–2873.
33 R. A. Marcus, *J. Chem. Phys.*, 1956, **24**, 966–978.
34 C.-P. Hsu, *Phys. Chem. Chem. Phys.*, 2020, **22**, 21630–21641.
35 W. Senevirathna, C. M. Daddario and G. Sauvé, *J. Phys. Chem. Lett.*, 2014, **5**, 935–941.
36 R. Chen, Y. Wang, T. Chen, H. Li, C. Zheng, K. Yuan, Z. Wang, Y. Tao, C. Zheng and W. Huang, *J. Phys. Chem. B*, 2015, **119**, 583–591.

37 M.-K. Yan, Y. Tao, R.-F. Chen, C. Zheng, Z.-F. An and W. Huang, *RSC Adv.*, 2012, **2**, 7860–7867.
38 J. Li, Z. Nie, H. Li, Y. Peng, Z. Wang, Z. Mai and W. Zheng, *J. Mater. Chem. C*, 2015, **3**, 4859–4867.
39 G. Velmurugan, S. Angeline Vedha and P. Venuvanalingam, *RSC Adv.*, 2014, **4**, 53060–53071.
40 G. Nan, X. Yang, L. Wang, Z. Shuai and Y. Zhao, *Phys. Rev. B: Condens. Matter Mater. Phys.*, 2009, **79**, 115203–115209.
41 J.-I. Park, B. L. Lee and J. W. Chung, Organic semiconductor compound, and transistor and electronic device including the same, US 20120168726 A1, 2012.
42 WO2007004799, 2007.
43 T. Kojima, R. Yokota, C. Kitamura, H. Kurata, M. Tanaka, H. Ikeda and T. Kawase, *Chem. Lett.*, 2014, **43**, 696–698.
44 K. Y. Cheung, K. Watanabe, Y. Segawa and K. Itami, *Nat. Chem.*, 2021, **13**, 255–259.
45 C. S. Frampton, K. S. Knight, N. Shankland and K. Shankland, *J. Mol. Struct.*, 2000, **520**, 29–32.
46 J. Hu, D. Zhang and F. W. Harris, *J. Org. Chem.*, 2005, **70**, 707–708.
47 R. B. Campbell, J. M. Robertson and J. Trotter, *Acta Crystallogr.*, 1962, **15**, 289–290.
48 M. Sola, *Front. Chem.*, 2013, **1**, 22.
49 E. Clar, *The aromatic sextet*, Wiley-Interscience, London, 1972.
50 A. D. Becke, *J. Chem. Phys.*, 1993, **98**, 5648–5652.
51 R. Ditchfield, W. J. Hehre and J. A. Pople, *J. Chem. Phys.*, 1971, **54**, 724–728.
52 J. D. Chai and M. Head-Gordon, *Phys. Chem. Chem. Phys.*, 2008, **10**, 6615–6620.
53 R. A. Kendall, T. H. Dunning and R. J. Harrison, *J. Chem. Phys.*, 1992, **96**, 6796–6806.
54 T. Stein, H. Eisenberg, L. Kronik and R. Baer, *Phys. Rev. Lett.*, 2010, **105**, 266802.
55 W. Schmidt, *J. Chem. Phys.*, 1977, **66**, 828–845.
56 J. V. Metzger, in *Comprehensive Heterocyclic Chemistry*, ed. A. R. Katritzky and C. W. Rees, Pergamon, Oxford, 1984, pp. 235–331.
57 J. L. Brédas, *Mater. Horiz.*, 2014, **1**, 17–19.
58 M. Gingras, V. Placide, J. M. Raimundo, G. Bergamini, P. Ceroni and V. Balzani, *Chem. – Eur. J.*, 2008, **14**, 10357–10363.
59 W. N. Hansen and G. J. Hansen, *Phys Rev A*, 1987, **36**, 1396–1402.
60 S. A. Odom, S. R. Parkin and J. E. Anthony, *Org. Lett.*, 2003, **5**, 4245–4248.
61 National Institute of Standards and Technology, NIST, **https://webbook.nist.gov**.
62 J. Chandrasekhar, J. G. Andrade and P. V. R. Schleyer, *J. Am. Chem. Soc.*, 1981, **103**, 5609–5612.
63 G. Malloci, G. Cappellini, G. Mulas and A. Mattoni, *Chem. Phys.*, 2011, **384**, 19–27.
64 G. Malloci, G. Mulas, G. Cappellini and C. Joblin, Chem. Phys., 2007, check, check.
65 G. Chen and R. G. Cooks, *J. Mass Spectrom.*, 1995, **30**, 1167–1173.
66 E. S. Chen and E. C. M. Chen, *Rapid Commun. Mass Spectrom.*, 2018, **32**, 230–234.
67 J. R. Platt, *J. Chem. Phys.*, 1949, **17**, 484–495.
68 Pyrene shows absorption maxima at 273 nm (log e = 4.77), 306 nm (log e = 5.07), 320 nm (log e = 4.51), 335 (log e = 4.78) in cyclohexane.
69 S. Shirai and S. Inagaki, *RSC Adv.*, 2020, **10**, 12988–12998.
70 E. L. Graef and J. B. L. Martins, *J. Mol. Model.*, 2019, **25**, 183.
71 R. A. Freidel and M. Orchin,*Ultraviolet Spectra of Aromatic Compounds*, John Wiley & Sons, Inc., New York, 1951.
72 J. Y. Hu, A. Paudel, N. Seto, X. Feng, M. Era, T. Matsumoto, J. Tanaka, M. R. Elsegood, C. Redshaw and T. Yamato, *Org. Biomol. Chem.*, 2013, **11**, 2186–2197.
73 N. J. Turro, V. Ramamurthy and J. C. Scaiano, Modern Molecular Photochemistry of Organic Molecules, University Science Books 2010.
74 J. Merz, J. Fink, A. Friedrich, I. Krummenacher, H. H. Al Mamari, S. Lorenzen, M. Haehnel, A. Eichhorn, M. Moos, M. Holzapfel, H. Braunschweig, C. Lambert, A. Steffen, L. Ji and T. B. Marder, *Chem. – Eur. J.*, 2017, **23**, 13164–13180.
75 R. L. Martin, *J. Chem. Phys.*, 2003, **118**, 4775–4777.
76 P. Kimber and F. Plasser, *Phys. Chem. Chem. Phys.*, 2020, **22**, 6058–6080.
77 H. F. Bettinger, C. Tönshoff, M. Doerr and E. Sanchez-Garcia, *J. Chem. Theory Comput.*, 2016, **12**, 305–312.
78 M. Pinheiro, L. F. A. Ferrão, F. Bettanin, A. J. A. Aquino, F. B. C. Machado and H. Lischka, *Phys. Chem. Chem. Phys.*, 2017, **19**, 19225–19233.
79 M. Pinheiro, Jr., A. Das, A. J. A. Aquino, H. Lischka and F. B. C. Machado, *J. Phys. Chem. A*, 2018, **122**, 9464–9473.
80 Y. Yang, E. R. Davidson and W. Yang, *Proc. Natl. Acad. Sci. U. S. A.*, 2016, **113**, E5098–E5107.
81 M. Pinheiro, F. B. C. Machado, F. Plasser, A. J. A. Aquino and H. Lischka, *J. Mater. Chem. C*, 2020, **8**, 7793–7804.
82 M. Malagoli, V. Coropceanu, D. A. da Silva and J. L. Brédas, *J. Chem. Phys.*, 2004, **120**, 7490–7496.
83 J. R. Reimers, *J. Chem. Phys.*, 2001, **115**, 9103–9109.
84 V. Coropceanu, O. Kwon, B. Wex, B. R. Kaafarani, N. E. Gruhn, J. C. Durivage, D. C. Neckers and J.-L. Brédas, *Chem. – Eur. J.*, 2006, **12**, 2073–2080.
85 R. A. W. Johnstone and F. A. Mellon, *J. Chem. Soc., Faraday Trans. 2*, 1973, **69**, 1155–1163.
86 M. Rossi and K. Sohlberg, *J. Phys. Chem. C*, 2009, **113**, 6821–6831.
87 A. Ruzsinszky, J. P. Perdew, G. I. Csonka, O. A. Vydrov and G. E. Scuseria, *J. Chem. Phys.*, 2006, **125**, 194112.
88 P. Mori-Sánchez, A. J. Cohen and W. Yang, *J. Chem. Phys.*, 2006, **125**, 201102.
89 R. Baer, E. Livshits and U. Salzner, *Annu. Rev. Phys. Chem.*, 2010, **61**, 85–109.
90 J. D. Chai and M. Head-Gordon, *Phys. Chem. Chem. Phys.*, 2008, **10**, 6615–6620.
91 R. W. I. de Boer, M. Jochemsen, T. M. Klapwijk, A. F. Morpurgo, J. Niemax, A. K. Tripathi and J. Pflaum, *J. Appl. Phys.*, 2004, **95**, 1196–1202.

92 M. J. Frisch, G. W. Trucks, H. B. Schlegel, G. E. Scuseria, M. A. Robb, J. R. Cheeseman, G. Scalmani, V. Barone, B. Mennucci, G. A. Petersson, H. Nakatsuji, M. Caricato, X. Li, H. P. Hratchian, A. F. Izmaylov, J. Bloino, G. Zheng, J. L. Sonnenberg, M. Hada, M. Ehara, K. Toyota, R. Fukuda, J. Hasegawa, M. Ishida, T. Nakajima, Y. Honda, O. Kitao, H. Nakai, T. Vreven, J. A. MontgomeryJr, J. E. Peralta, F. Ogliaro, M. J. Bearpark, J. Heyd, E. N. Brothers, K. N. Kudin, V. N. Staroverov, R. Kobayashi, J. Normand, K. Raghavachari, A. P. Rendell, J. C. Burant, S. S. Iyengar, J. Tomasi, M. Cossi, N. Rega, N. J. Millam, M. Klene, J. E. Knox, J. B. Cross, V. Bakken, C. Adamo, J. Jaramillo, R. Gomperts, R. E. Stratmann, O. Yazyev, A. J. Austin, R. Cammi, C. Pomelli, J. W. Ochterski, R. L. Martin, K. Morokuma, V. G. Zakrzewski, G. A. Voth, P. Salvador, J. J. Dannenberg, S. Dapprich, A. D. Daniels, Ö. Farkas, J. B. Foresman, J. V. Ortiz, J. Cioslowski and D. J. Fox, *Gaussian, Inc.*, Wallingford, CT, USA, 2009.
93 N. M. O'Boyle, A. L. Tenderholt and K. M. Langner, *J. Comput. Chem.*, 2008, **29**, 839–845.
94 H. Ma, N. Liu and J.-D. Huang, *Sci. Rep.*, 2017, **7**, 331.
95 C.-R. Zhang, V. Coropceanu, J. S. Sears and J.-L. Brédas, *J. Phys. Chem. C*, 2014, **118**, 154–158.
96 NIST Computational Chemistry Comparison and Benchmark Database, NIST Standard Reference Database Number 101 Release 22, **https://cccbdb.nist.gov/**, Accessed April 2024, 2024.